Tactile On-Chip Pre-Processing with Techniques from Artificial Retinas

R. Maldonado-López[a], F. Vidal-Verdú[b], G. Liñán[a], E. Roca[a] and A. Rodríguez-Vázquez[a]
[a]Dept.of Analog and Mixed-Signal Circuit Design. IMSE-CNM-CSIC, Edificio CICA, Avda. Reina Mercedes s/n, 41012-Sevilla, SPAIN, angel@cnm.us.es
[b]Dto.Electrónica-Universidad de Málaga. Complejo Tecnológico, Campus Teatinos 29071 Málaga, SPAIN, vidal@ctima.uma.es

ABSTRACT

The interest in tactile sensors is increasing as their use in complex unstructured environments is demanded, like in telepresence, minimal invasive surgery, robotics etc. The matrix of pressure data these devices provide can be managed with many image processing algorithms to extract the required information. However, as in the case of vision chips or artificial retinas, problems arise when the array size and the computation complexity increase. Having a look to the skin, the information collected by every mechanoreceptor is not carried to the brain for its processing, but some complex pre-processing is performed to fit the limited throughput of the nervous system. This is specially important for high bandwidth demanding tasks. Experimental works report that neural response of skin mechanoreceptors encodes the change in local shape from an offset level rather than the absolute force or pressure distributions. This is also the behavior of the retina, which implements a spatio-temporal averaging. We propose the same strategy in tactile preprocessing, and we show preliminary results when it faces the detection of the slip, which involves fast real-time processing.

Keywords: tactile sensors, slip detection, bioinspired chips

1. INTRODUCTION

Tactile sensors emulate the human skin behavior to collect the information provided by the normal and tangential forces on its surface and their changes along time. Although many of them have been reported and fabricated, these devices have had a slow development specially because of the lack of knowledge about the sense of touch and of applications that push the research into this area [1]. Generally speaking, the smart sensors are intended to operate in complex, poorly structured environments. This kind of applications has become recently common and will be much more present in the future [2], for instance in medicine, where Minimal Invasive Surgery requires tactile sensors and displays for the surgeon to touch inside the patient through a small hole. They are also useful in rehabilitation of damaged hands, or can be part of advanced aids for blind people, elder people, or others that have lost sensitivity in parts of their bodies. Tactile sensors are also of great interest for food processing industry, where fragile or soft objects could be manipulated at low temperatures. Finally, telepresence and Virtual Reality are also application areas for these devices where much work is being carried out.

Ideally, a tactile sensor should be able to provide information about texture, stiffness, slippage, friction, local shape, etc. Real devices are usually arrays of force sensors whose output is a tactile image that can be processed with common algorithms for visual images. Most of them are based on piezoresistive or capacitive transduction. The piezoresistive sensors exploit the dependence of the electrical resistance on mechanical deformation. Many of them are made of elastomers or polymers that cover an array of electrodes or are part of a multilayer flexible structure [3][4][5]. These sensors are simple but they have poor stability with time and temperature, they have hysteresis and low linearity. Other devices are based on MEMS technologies, and basically are small mesas that are supported by cantilevers made of piezoresistive material [6][7]. They can be modified easily to detect also tangential forces [8] and are very linear, but less sensitive than capacitive sensors. Capacitive tactile sensors exploit the dependence of the capacitance on the area or distance between the electrodes, or on the permittivity of the dielectric. The latter is used to detect changes in human tissues in medicine, or to build chips that read the human fingerprint. Most capacitive tactile sensors exploit the dependence on distance between the electrodes [9][10], their response is not as linear as in the resistive case and they are not easily adapted to detect tangential forces, but they are more sensitive and more robust against temperature variations. Finally, other tactile sensors are based on optical

Bioengineered and Bioinspired Systems II, edited by Ricardo A. Carmona, Gustavo Liñán-Cembrano, Proceedings of SPIE Vol. 5839 (SPIE, Bellingham, WA, 2005)
0277-786X/05/$15 · doi: 10.1117/12.607605

principles or on piezoelectric materials [1].

The above described sensors are basically arrays that do not implement any on-chip processing. Some implement the signal conditioning circuitry in the same substrate [10][11], which is a first step to reduce the errors and easy the reading of dense arrays. This first step is possible due to technologies that allow the implementation of the sensor and the circuitry in the same substrate. This preprocessing could not be interesting if small arrays are implemented and real time response is not required. However, if they are dense matrixes or fast response is needed a preprocessing able to compact the information collected by the cells to be properly conveyed to a central decision making unit is mandatory. A task that fits this scenario is the slip detection. It consists in the early notification of the slip of an object while being manipulated by a robot. This detection is specially critical if fragile objects are handled. In this case, if the robot hands or grippers exert a too strong grasp force on the object it could be damaged, but it could slip and fall if the force is too weak. Moreover, the slip of the object should not be confused with a rolling condition that could be normal in the manipulation process.

In the case of a translation, the slip takes place if the following condition fulfils:

$$\frac{f_t}{f_n} \leq \mu \tag{1}$$

where μ is the friction coefficient, and f_t and f_n are the tangential and normal forces at the contact area. A strategy to detect slip is based on (1). However, this method requires the measurement or estimation of the friction coefficient, which is a very difficult task to do in a general case because μ varies depending on the grasp force and the grasp configuration [12]. Moreover, in the case of a rotation plus translation movement, the slip condition depends on the distribution of normal and tangential stress in the contact interface [4][13][14]. Some implementations trains an artificial neural network to be able to detect slip under different conditions without an explicit estimation of μ, but the results are limited because of the large number of variables involved, like surface shape and nature, load weight, different indenters, different load increment stories, different positions, etc.[13][15] Other approaches use more sensors to detect slip, like cameras, joint encoders and fingertip force/torque sensors [12][[4] and follow quite complex algorithms that still take some assumptions like a certain shape of the manipulated object.

Another approach is based on the detection of microvibrations that happen once the slippage occurs. These vibrations are generated by the sequence of stick-slip cycles during the slip, when the surface at the contact area between the indenter and the manipulated object stretches (stick) until the slip condition (1) fulfils and then snaps back (slip). Dynamic sensors or accelerometers can be used to detect such vibrations [14][16]. However, this can be an error prone method due to the interference of environmental vibrations as those generated in the course of multi finger manipulation [13]. Moreover, the robot fingertip cannot house many devices without causing mechanical interference with one another [17]. Finally, these microvibrations are localized in the peripheral area of the contact [17], which suggests the use of many dynamic devices instead of just one to get a more early and reliable detection.

In the biological world, human skin relies on mechanoreceptors in the skin to detect slip [16]. Specifically, signals from the fast adapting FA nerve endings indicate the earliest stages of slip [14] which are followed by an unconscious increase in the grasp force to prevent further slippage. Some proposals implement a kind of artificial skin based on piezoelectric film PVDF sensors [17][18] in a sort of distributed dynamic sensor. An ANN (Artificial Neural Network) is trained in [17] to give a slippage condition signal even when noise is added. However, these sensors do not provide other static tactile information like pressure distributions. It would be desirable to have a tactile sensor capable to give as much information as possible. Reference [3] reports a work in which a simple tactile sensor that gives the pressure distribution as output is used to detect slip. Again, an ANN is used in the best approach to get robustness under uncertainty or noise. The algorithm is complex because it requires the computation of the FFT besides of other calculi, thus it needs powerful and fast hardware.

In this paper, we propose a different approach that is inspired in the human skin but also in its similarities with the retina. As said above, the tactile sensor output is in fact a tactile image that shows a map of distributed pressures, and it can be processed by algorithms intended for visual images. If real time processing is needed, we could still exploit resources developed for visual images, like those implemented in artificial retinas. Specifically, these retinas are able to detect motion, and this capability can be adapted in the case of a tactile sensor to detect slip. Moreover, artificial retinas implement a spatio-temporal averaging that provide an automatic gain control that extends the useful operating range. This procedure is inspired in the way the biological retina works. The human retina is sensitive to changes in its input, no matter what the viewing conditions [19]. It has been observed that the skin also has a similar behavior, and neural response of skin mechanoreceptors encodes the change in local shape from an offset level rather than the absolute force or pressure distributions [20]. The sensitivity to local instead of global variations makes the skin able to sense features in very irregular objects or

surfaces with different textures. Specifically, a slip condition is detected when very different objects are manipulated.

2. ARCHITECTURE

As said above, we are interested in slip detection as a first problem to solve and explore the power of vision hardware resources in the tactile field. A first step could be the use of the architecture of the silicon retina described in [19]. It could be valid to detect slip since it is sensitive to changes in the signal from the visual sensors corresponding to movements, for instance sudden movements like those produced by a predator in the shadow, which has a clear counterpart in the detection of slip under different conditions like load weight or indenters.

Fig.1. shows the architecture. A single tactel element is illustrated in the circular window. The resistive network computes a spatio-temporal (taking into account the capacitors) average of the signals provided by the follower-connected transconductance amplifier by which the force sensor drives it. The spatial scale of the weighting function depends on the product of the lateral resistance R and the conductance of the follower-connected amplifier G, and the larger the distance between two nodes, the lower the influence on each other. A second amplifier senses the difference across the conductance G, that is the difference between the sensor output and the voltage at the corresponding network node. This processing enhances the edges in the image. Moreover, it allows a gain control on the sensor output that takes the spatio-temporal average as a reference. A first consequence is that the array is able to operate under very different situations corresponding to different maps of normal pressure detected by the tactile sensor. Specifically, it is able to detect small changes in an input with respect to the surrounding area defined by the spatial scale of the network.

Another important aspect of this network is its dynamic behavior. The capacitor associated to every node in the network implements a delay that could be characterized by the time constant $\tau = C/G$. The output amplifier responds to changes of the sensor signal with respect to the network node voltage stored in the capacitor, which enhances the moving images. In other words, the circuit implements a spatio-temporal high-pass filter. This feature can be exploited to detect the microvibrations produced by slip if the circuit dynamic response is properly tuned. This is what we have done in this paper, where we also have used a comparator as high gain amplifier at the output stage of the retina node. Microvibrations are notified by a train of pulses with an amplitude determined by the output range of the comparator and a frequency determined by the frequency of the slip vibrations. If just a slip condition signal is required, a kind of logic OR connection (open collector) to a single line can be implemented for every node. It is important now to be aware of the dynamic requirements of the circuitry to detect slip, specifically what are the main components in the frequency spectrum of a stick-slip signal.

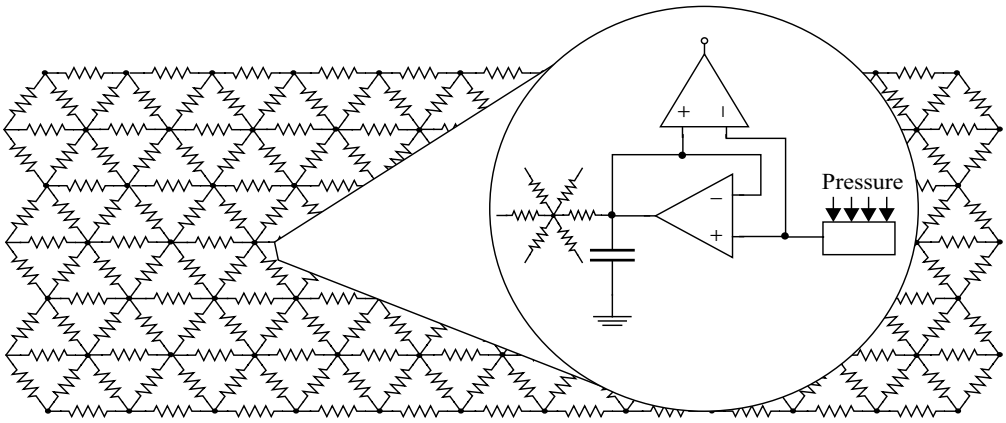

Fig.1. The proposed architecture is that of the retina reported in [19].

3. STICK-SLIP SIGNAL FREQUENCY BEHAVIOR

Fig.2.(a) shows a simple experimental set-up that has been used to obtain a slip signal and know its dynamic behavior. A conductive rubber has been placed on a PCB board with a few parallel copper strips. The resistance of the rubber (Zoflex@ZL45.1) depends on the pressure exerted on it. If a constant current is injected between two strips, the voltage drop between these electrodes will be a measurement of the pressure right in the electrodes location. A DC motor has been used to produce a sustained slip condition. A rubber wheel in the motor axis is forced to slip on the resistive rubber at the elec-

trodes location, and the voltage drop is measured with a scope. Since the rubber resistance has a non linear dependence on the pressure, output changes in the voltage are quite large sometimes. In addition, the rubber wheel is not a perfect circle, actually it has eccentricities where the stick-slip response is detected.

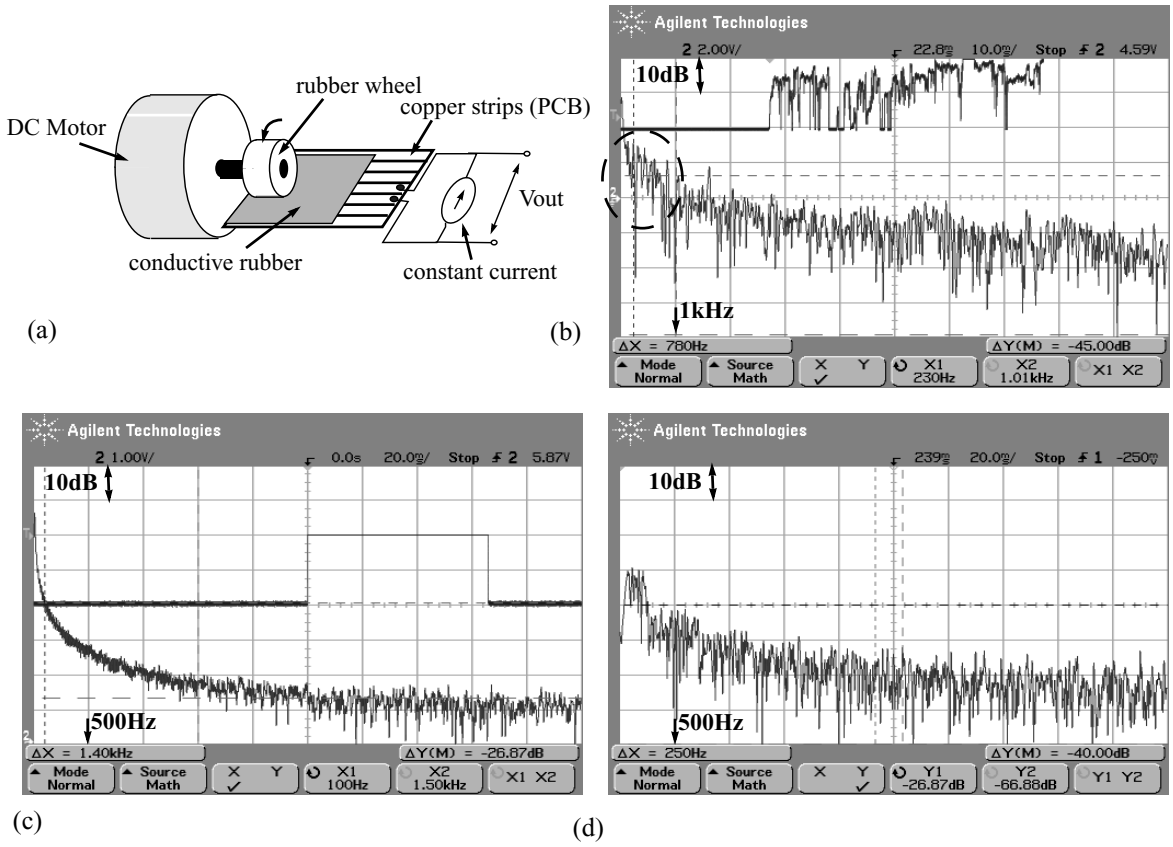

Fig.2. Simple experimental set-up to know the frequency response of the slip.

Fig.2.(b) shows the signal versus time (top) and its FFT as obtained from the scope (bottom). It can be observed that there is a significant response between 60 and 220Hz approximately, where the output is attenuated around 15dB with respect to the dc level. This result is coherent with observations from other authors [3][17]. It is also worthy to mention that the FA mechanoreceptors in the human skin has a maximum sensitivity also in this frequency range [16].

The response to a rolling condition right in a sensor of the tactile array has also measured and the result is shown in Fig.2.(c), where again the output signal is at the top of the figure while its FFT is at the bottom. Note the difference between Fig.2.(b) and Fig.2.(c) at the frequencies 60- 220Hz.

Taking into account the sharp nature of the changes in the stick-slip sequence, as observed also experimentally, and the knowledge of the frequency range of interest, a possible model of the slip microvibrations to be used in our simulations could be a frequency modulated square signal. Such signal has the spectrum in Fig.2.(d), where the modulation signal is a linear ramp. The obtained spectrum is quite similar to that in Fig.2.(b) for the measured slip signal. During slip, normal force usually does not change much [3] (large variations in Fig.2.(b) are caused by the quite low linearity of the conductive rubber).

4. BUILDING BLOCKS

From the point of view of the dynamic response, which is our initial aim, the requirement for Fig.1. is being sensitive to the frequency range of the slip specified in section 3. Since minimum frequencies to be detected are around 60Hz, this means that the time constant $\tau = C/G$ must be very large. We need then a large capacitance and a very small transconductance of the follower-connected OTA. Both goals can be got if we use previously reported techniques to implement

very low frequency OTA-C filters [21][22].

4.1. Implementation of a large capacitance

Capacitors are implemented on integrated circuits in many different ways, but they consume a large area if the capacitance is big. An impedance scaler circuit can be used instead to get the desired high capacitance value while saving area. Two main approaches to scale the impedance of a grounded capacitor are depicted in Fig.3. The strategy in Fig.3.(a) is

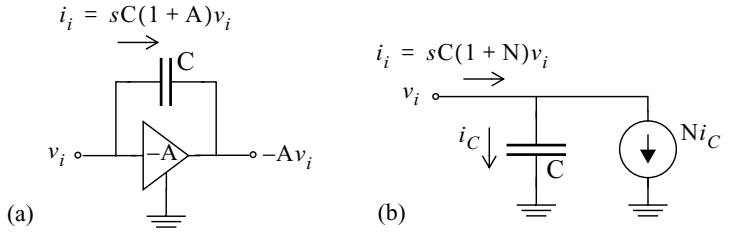

Fig.3. Impedance scalers: (a) based on voltage amplification, (b) based on current amplification.

based on voltage amplification. It can be implemented with a simple inverter as amplifier. The drawback of this choice is the trade-off between input range and gain A it presents. We have made simulations with this scaler successfully, but it is difficult to keep it in the proper range of operation. A more robust circuit in that sense is based on current amplification, as Fig.3.(b) illustrates.

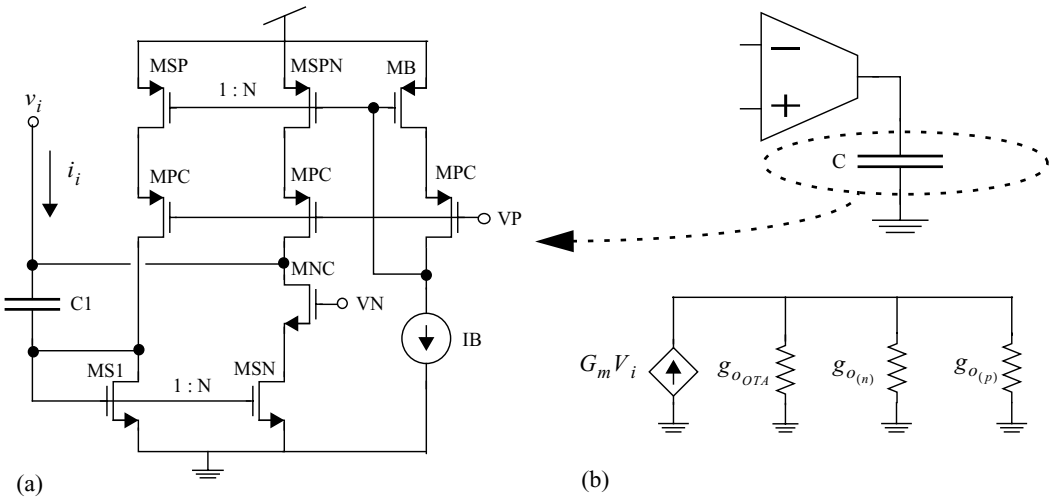

Fig.4. Impedance scaler circuit (a) and simple small signal model of a filter with this circuit (b).

Fig.4. shows such circuit as we have implemented it in the architecture of Fig.1. The so obtained impedance is

$$Z_i = \frac{v_i}{i_i} \approx \frac{1}{s(N+1)C} \tag{2}$$

where it has been supposed that the transconductance g_{mn} of the nmos transistors is very high when compared to $g_{o(n)}$, $g_{o(p))}$ (output conductance of the *n* and *p* branches in Fig.4.) and *sC*. As equation (2) states, the larger the value of *N*, the higher the final impedance value. However, the dc gain of the obtained filter is

$$A_{dc} = \frac{G_m}{g_o + N(g_{o(p)} + g_{o(n)})}, \tag{3}$$

which degrades with *N*. In order to increase the dc gain and reduce systematic errors, cascode transistors have been added in the output branches of the scaler. The output resistance of these branches is increased this way, and the denominator in (3) decreases.

Fig.5. shows the frequency response at the output of the follower connected OTA for different values of N, when using a bias current I_b = 10nA for the OTA and a capacitor value of C1=5pF. In order to detect slip, the cutoff frequency must be around 60Hz. To accomplish this specification, N value of 8 has been finally chosen.

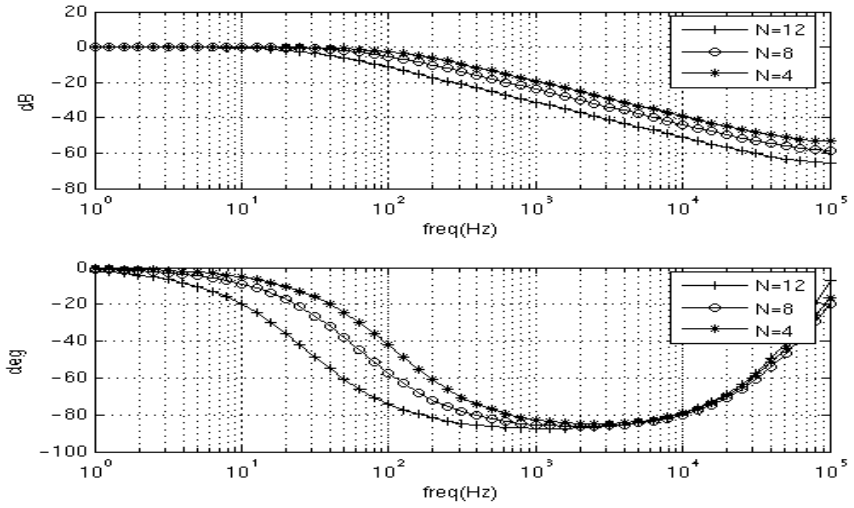

Fig.5. Frequency response for different values of N.

4.2. Follower connected OTA

As said above, very small transconductance OTAs are required to get a small time constant and detect slip. Three main design keys have been followed for that purpose: pmos differential pair as core, current division and source degeneration.

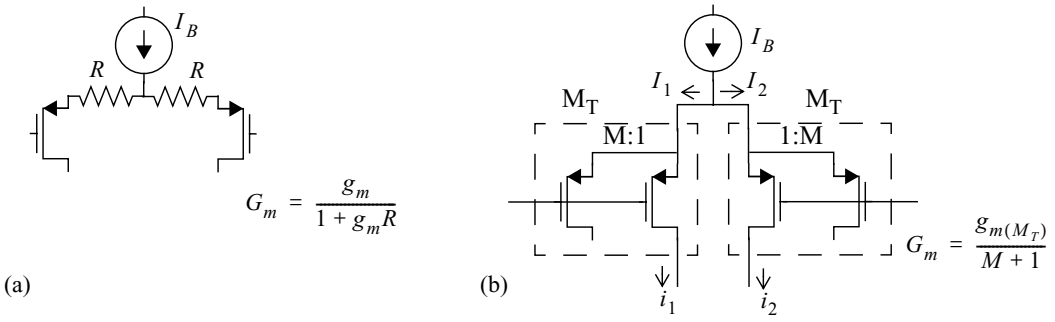

Fig.6. Strategies to reduce the OTA transconductance: (a) source degeneration and (b) current division.

First, the use of a pmos differential pair as OTA core instead of a nmos differential pair reduces the transconductance because of the lower mobility of holes when compared to electrons, which translates into lower transconductance of the pmos devices. Second, a common strategy to increase linearity and input range while reducing the OTA transconductance consists in the use of resistors to degenerate the source of the transistors in the differential pair (see Fig.6.(a)). These resistors can be implemented with transistors in the linear operating region. Finally, the current division principle consists in reducing the current in the transconductor by splitting it. For instance, in the differential pair at Fig.6.(b) the currents I_1 and I_2 in both sides are splitted into M+1 identical parts, and just one of these parts per side, i_1 and i_2 in Fig.6.(b), is used for further processing in the OTA. Since the current is divided, the resulting transconductance is also divided by a similar factor. Fig.7. depicts the OTA implemented in our paper, which has been proposed in [21] to be used to build very low frequency filters. The resistor R in Fig.6. is realized in Fig.7. with a transistor in the triode region. The so obtained OTA transconductance is [22]

$$G_M = \frac{g_{m(M_i)}}{1 + \dfrac{(M+1)g_{m(M_i)}}{g_{o(M_R)}}} \tag{4}$$

where

$$g_{o(M_R)} = n\mu C_{0x}\frac{W_{M_R}}{L_{M_R}}\sqrt{\frac{2I_b L_{M_C}}{n\mu C_{0x} W_{M_C}}} \tag{5}$$

is the conductance of the transistor MR. Note that this conductance is controlled by the bias current I_b. Thus, the OTA transconductance in (4) is also controlled by this current.

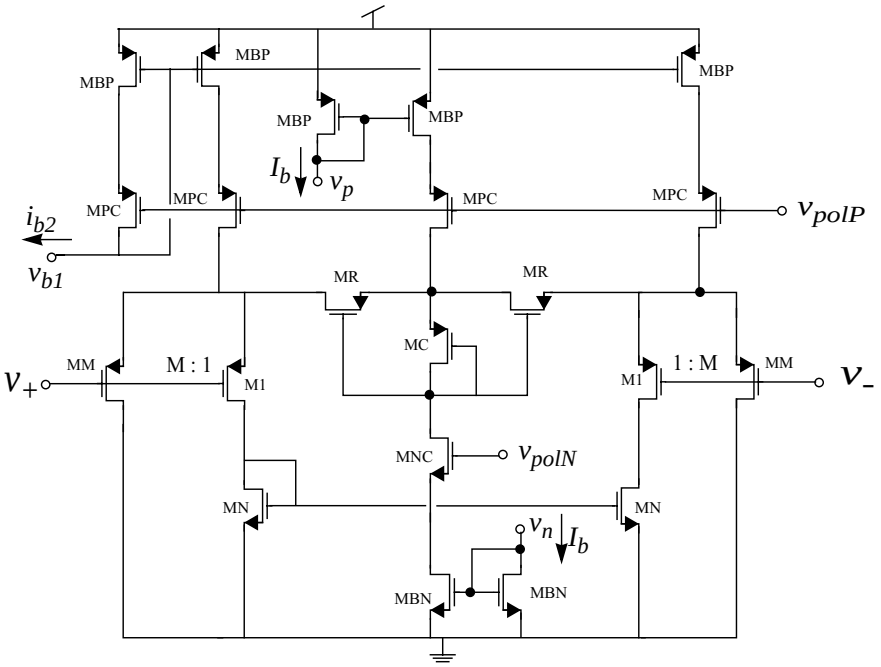

Fig.7. Very low transconductance OTA [21].

Other strategies to reduce the transconductance use floating gate transistors or bulk driven transistors as input transistors in the OTA. However, the OTA in Fig.7. has a better performance, specially in terms of area consumption [22].
Fig.8. shows the frequency response at the output of the follower connected OTA for different values of I_b, when using a N value of 8 for the impedance scaler gain and a capacitor value of C1=5pF. To obtain a suitable cutoff frequency around

60Hz, a value of I_b =10nA has been chosen.

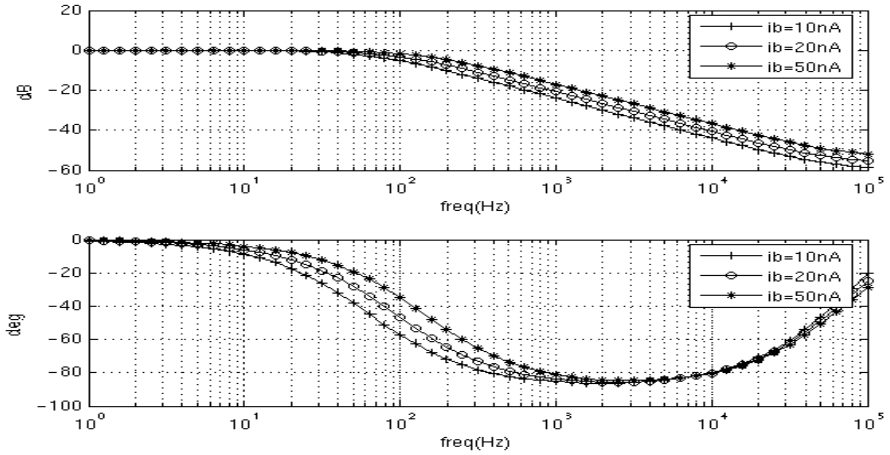

Fig.8. Frequency response for different values of I_b .

4.3. Network resistors.

The resistors in the array of Fig.1. have been implemented in this paper like those described in the previous section to degenerate the sources of transistors in the OTA. This consumes much less area than a network made of passive resistors, for instance polisilicon resistors. Moreover, it is also simpler than the horizontal resistor (HRes) reported in [19]. For the sake of clarity, Fig.9. shows the implementation of every resistor in the array as well as the associated resistance. Note that the resistor is composed of two transistors and their gate voltage is related to the common node, which reduces the sensitivity to changes in the common mode input voltage [21].

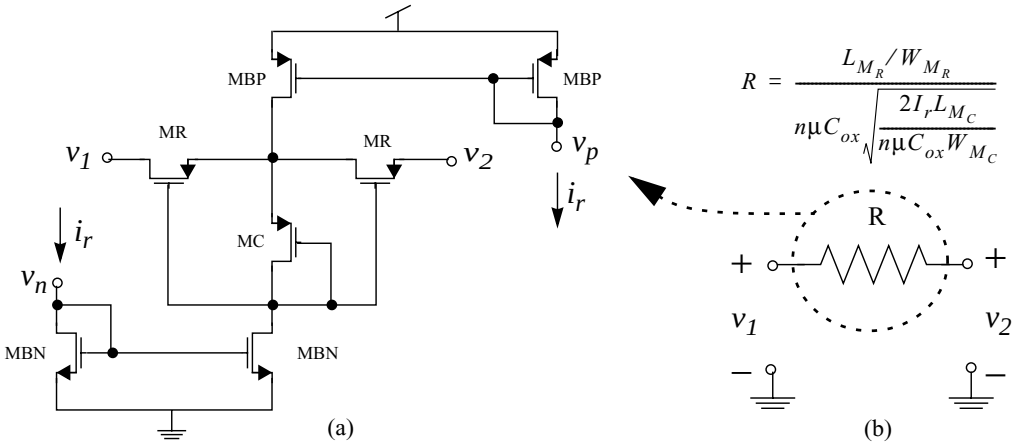

Fig.9. Implementation of Network Resistor (a) and its associated resistance (b).

4.4. Comparator.

Mead's retina nodes consist of the input sensor (a pressure sensor in our case), a capacitor, a follower connected amplifier and a second amplifier, which senses the voltage difference across the conductance provided by the first amplifier and generates the output of each cell. A comparator is placed at the output stage of our tactile sensor as output amplifier. This block takes the variation between the pressure sensor output and the weighted average of the potentials of surrounding points in the tactile image stored on the capacitor. However, instead of an analog value related to local input pressure we obtain a kind of digital signal, because microvibrations of the sensor output signal, in the range of the frequencies related

to slip, will cause the output signal to oscillate from high to low state, thus generating the train of pulses mentioned in section 2. A second amplifier could be added to obtain the information related to local pressure.

The results of this paper have been obtained with a Verilog macro generated by Cadence Modelwriter as comparator. The model corresponds to a comparator with discontinuity removed by using a tanh transfer function. It has hysteresis and slew rate limiter.

5. RESULTS

In order to evaluate the performance of the architecture proposed in this paper, and to check its efficiency in detecting the slip or the rolling condition, a set of simulations has been carried out. Stimulus corresponding to these phenomena have been modeled and applied to different arrays based on the architecture shown in Fig.1. Finally, results from transient simulations of a 1-dimension-10-cell tactile sensor are presented and discussed.

5.1. Local Average Array and Global Average Array.

One of the characteristics of the architecture we propose in this paper is the use of a spatio-temporal average. We presume that it is an advantage when the problem of slip detection is faced. To highlight this idea, we have considered two types of arrays in our simulations, as shown in Fig.10. One of these uses a local average and the other one a global average. Thus, a comparative between the behavior of these arrays when they are used for slip detection have been made, and the obtained conclusions are commented in this section.

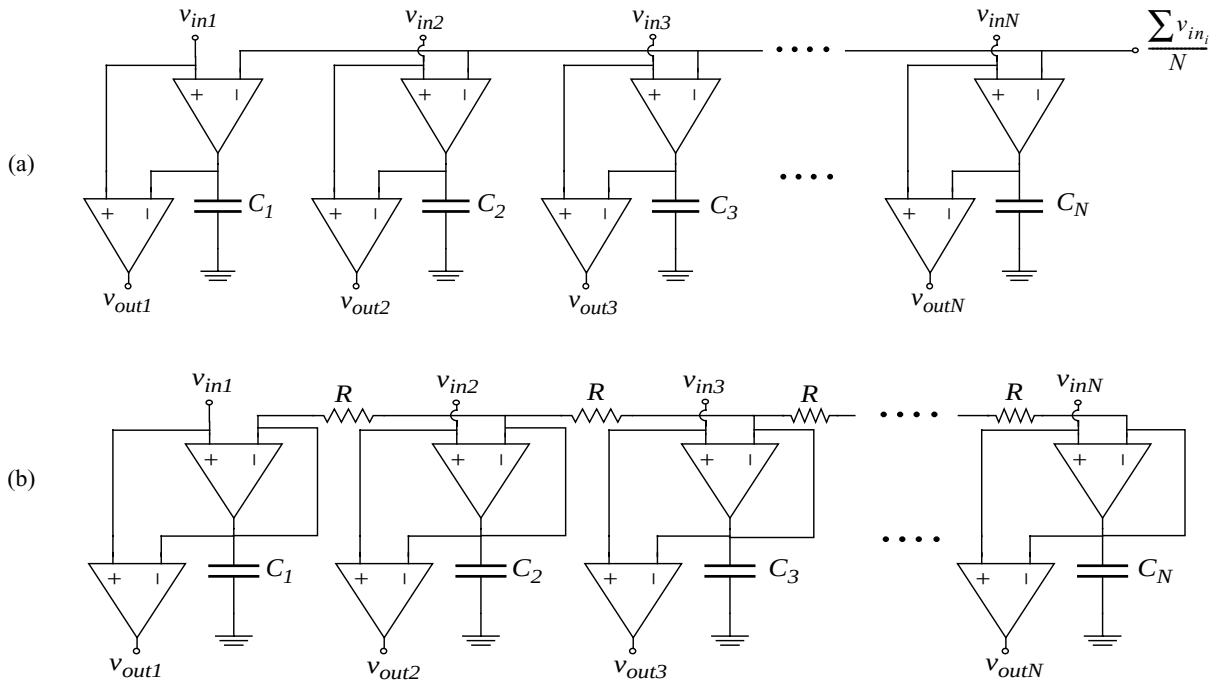

Fig.10. Global average array (a) and local average array (b).

5.2. Stimulus model.

An important step to obtain the preliminar results presented in this paper was to have proper stimulus. The experimental setup described in section 3 allowed us to know useful data about the frequency response and the temporal behavior of the two phenomena we are studying. Our stimulus model is based mainly in this experimental information as well as in reported experimental data. In order to achieve more complete results, we are interested in testing how different indenter shapes (thus, different pressure distribution shapes) could influence our tactile sensor behavior. Unfortunately, due to hardware

limitations, it has not been possible yet to get our experimental tactile sensor outputs corresponding to different indenters. Hence, we have completed our model with information presented in [13]. We have considered different indenter shapes: flat (4 mm wide), cylindrical (radius 10 mm) triangular (edge angle 120º), and parabolic.

Our transient simulations are divided in three different phases. At the beginning, no pressure is applied to the array. In the second phase, the indenter is pressed centered on the tactile sensor, but still does not move. Finally, the object begins to move, taking place the slip or the rolling condition, depending on the case.

Fig.11. shows an example of the stimulus applied to the cell at x=6, of a 1 dimension-10 node array, corresponding to the rolling condition. As we explained above, it is based on the observed response illustrated in Fig.2.(c), complemented with the different normal stress maps presented in [13] for three different indenters.

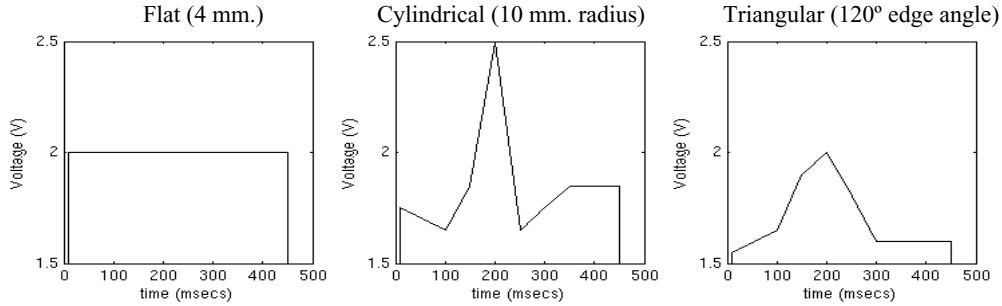

Fig.11. Stimulus model for different indenters [13].

A similar method has been used to model the slip stimulus, as shown in Fig.12. In this case, microvibrations due to slippage have been modeled by a linear frequency modulated square signal, according to the experiments described in section 3, but we have considered smaller variations than those observed when using the conductive rubber. Furthermore, a random component has been added to our vibrations model, taking into account possible noise efects.

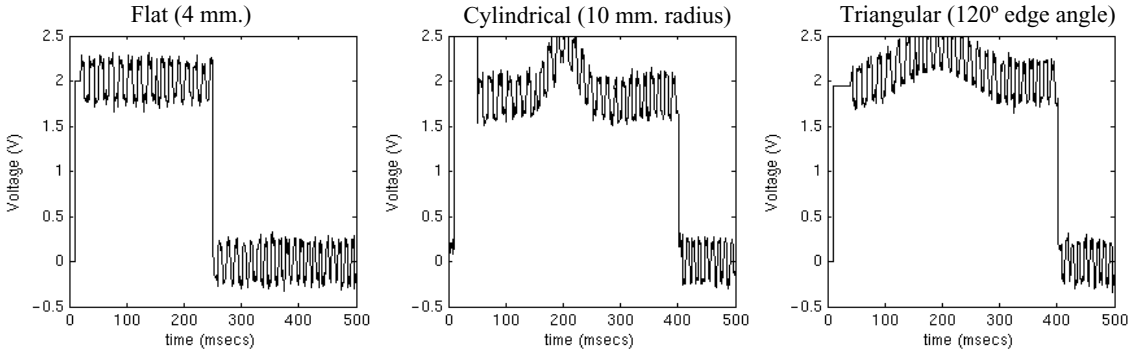

Fig.12. Stimulus model

5.3. Simulation Results.

In this section, obtained results from transient simulations of a 1 dimension-10-cell retina are presented. Inputs are different indenters rolling or slipping at constant speed of 20 tactels/sec. Fig.13 shows some examples of rolling condition simulations. Fig.14 illustrates examples of simulations for slippage. Outputs are shown for the cell at x=6.

It may be easily seen that the output signals provided by both retinas are clearly different for each situation, rolling condition (Fig.13) or slippage (Fig.14). The possibility of easy discrimination between these phenomena, could represent and important feature for some applications, as explained in section 1.

In all the cases, the initial pressure exerted by the indenter, from the moment the indenter is pressed above the array but before any other phenomena take place, forces a high logic output. Thus, this phase can be identified as a step at the beginning of our simulations.

When considering only rolling condition(Fig.13), during the motion of the object, outputs depends strongly on the indenter shape, and we haven't found a regular pattern which allow us to recognize this stage accurately. Besides, in some

cases the observed output corresponding to this stage is zero.

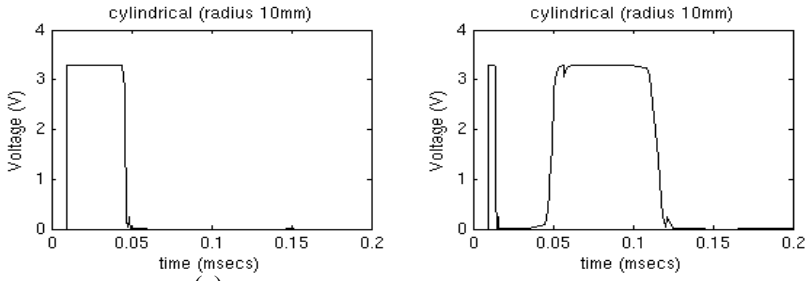

(a) (b)

Fig.13. Simulation results at x=6 for rolling condition. global average sensor (a) and local average sensor (b)..

In the case of slippage (Fig.14), it is clearly observed the difference in behavior between the two types of tactile sensors we have studied. The slip is, in fact, only detected when using the local average retina. Microvibrations are then advised by a train of pulses. The train of pulses is better-conformed, more continuous and wider in the case of flat indenters than for triangular or cylindrical indenters. For instance, in the simulation example shown in Fig.14.(b) for a cylindrical indenter, microvibrations due to the incipient slip are masked at the output of this specific cell of the array, but they are detected in the neighboring cells.

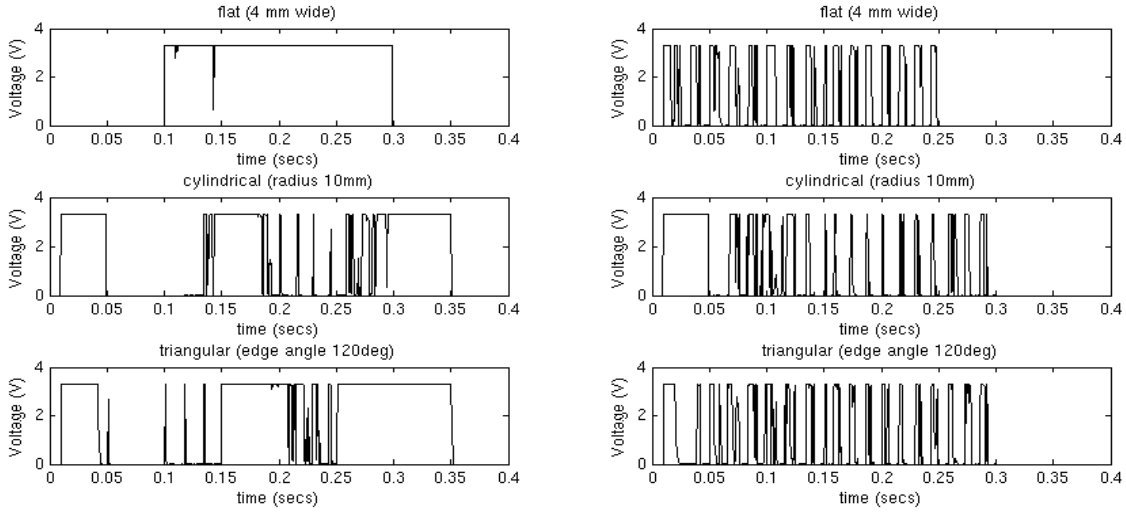

(a) (b)

Fig.14. Simulation results at x=6 for slip. global average retina (a) and local average retina (b).

6. CONCLUSIONS

This paper is intended to propose a new strategy to detect slip as an example of how resources developed for artificial retinas and vision chips can be used also to increase the capability of tactile sensors. Despite this is a first step, the simulation results show that this approach, and specifically the use of a similar architecture than that reported in [19], is able to detect the slip as we have modeled it even when different indenters are used. We have designed the building blocks to be able to detect very low frequency signals like those generated by the slip. However, since the architecture takes the local average as reference, its performance will depend on how much this average changes in the tactile image. For images corresponding to large pressure gradients, for instance due to triangular indenters, the difference between the sensor node output and the local average is large and it could mask the oscillations produced by the slip. In the case of indenters that produce quite uniform areas in the tactile image (although they correspond to very different pressures), for instance indenters with a square or parabolic profile, the local average is closer to the sensor node output and the spatial variations do not mask the temporal ones, hence the slip is clearly detected. Obviously, this will depend on the density of sensors in the array with respect to the pressure gradient. The results in this paper are preliminar, and more experimental data should be col-

lected to confirm and tune the design of the slip sensor. However, they show the feasibility of the proposal and encourage us to carry on this way.

ACKNOWLEDGMENTS.

This work has been partially funded by project TIC2003 - 09817-C02, and has been motivated from researcher exchanges from Sevilla and Málaga. The authors thank the contribution of ZOFLEX® for providing samples of pressure-activated conductive rubber sheets.

REFERENCES

1. M.H. Lee and H.R Nicholls, *Tactile sensing for mechatronics-a state of the art survey*, Mechatronics, Vol. 9, 1999.
2. M.H. Lee, *Tactile Sensing, New Directions, New Challenges*, The International Journal of Robotics Research, 2000.
3. E.G.M. Holweg, H. Hoeve, W. Jongkind, L. Marconi, C. Melchiorri, C. Bonivento, *Slip Detection by Tactile Sensors: Algorithms and Experimental Results*, Proc. of the 1996 IEEE International Conference on Robotics and Automation, Minneapolis, Minnesota, April 1996.
4. C. Melchiorri, *Slip Detection and Control Using Tactile and Force Sensors*, IEEE Transactions on Mechatronics, 2000.
5. M. Shimojo, R. Makino, A. Namiki, M. Ishikawa, T. Suzuki, K. Mabuchi, "A Sheet Type Tactile Sensor using Pressure Conductive Rubber with Electrical-Wires Stitches Method", *IEEE Sensors*, Orlando, 2002.
6. J. Engel, J. Chen and Ch. Liu, *Development of polyimide flexible tactile sensor skin*, Journal of Micromechanics and Microengineering, Vol. 3, pp.359-366, February 2003.
7. T. Lomas, A. Tuantranont and V.M. Bright, *Micromachined Piezoresistive Tactile Sensor Array Fabricated by Bulk-etched MUMPs Process*, NSTI Nanotechnology Conference, 2004.
8. B. J. Kane, M. R. Cutkosky and G. T. A. Kovacs, *A Traction Stress Sensor Array for Use in High-Resolution Robotic Tactile Imaging*, Journal of Electromechanical Systems, Vol. 9, No 4, December 2000.
9. T. Salo, T. Vancura, O. Brand, H. Baltes, *CMOS-Based Sealed Membranes for Medical Tactile Sensor Arrays*, IEEE MEMS, pp. 590-593, Kyoto, Japan, January 19. -23, 2003.
10. M. Leineweber, G. Pelz, M. Schmidt, H. Kappert, G. Zimmer, *New tactile sensor chip with silicone rubber cover*, Sensors and Actuators, Vol. 84, pp. 236-245, 2000.
11. U. Paschen, M. Leineweber, J. Arnelung, M. Schmidt, G. Zammer, *A Novel Tactile Sensor for Heavy-Load Applications Based on an Integrated Capacitive Pressure Senso*r, Sensors and Actuators, Vol. 68, pp. 294-298, 1998.
12. T. Hasegawa and K. Honda, *Detection and Measurement of Fingertip Slip in Multi-fingered Precision Manipulation whit Rolling Contact,* Journal of Robotics Society of Japan, Vol. 19, No. 7, pp 113-119. October 2001.
13. G. Canepa, R. Petrigliano, M. Campanella and D. De Rossi, *Detection of Incipient Object Slippage by Skin-Like Sensing and Neural Network Processing*, IEEE Transactions on Systems, man, and Cybernetics-Part B: Cybernetics, 1998.
14. R.D. Howe, *Tactile Sensing and Control of Robotic Manipulation*, Journal of Advanced Robotics, Vol. 8, 1994.
15. K. Hosoda, Y. Tada, and M. Asada, *Internal Representation of Slip for a Soft Finger with Vision and Tactile Sensors*, Proceedings of the 2002 IEEE/RSJ Conference on Intelligent Robots and Systems, Switzerland, October 2002.
16. R.D. Howe, M.R. Cutkosky, *Sensing Skin Acceleration for Slip and Texture Perception*, Proc. IEEE Robotics Automation, 1989.
17. I. Fujimoto, Y. Yamada, T. Morizono, Y. Umetani, T. Maeno, *Development of Artificial Finger Skin to Detect Incipient Slip for Realization of Static Friction Sensation*, IEEE Multisensor Fusion and Integration for Intelligent Systems, 2003.
18. Y. Yamada, H. Morita, and Y. Umetani, *Vibrotactile Sensor Generating Impulsive Signals for Distinguishing Only Slipping States*, Proc. of the 1999 IEEE/RSJ International Conference on Intelligent Robots and Systems, 1999.
19. C. Mead, *Analog VLSI and Neural Systems*, Addison-Wesley, 1989.
20. W. J. Peine and R. D. Howe, *Do Humans Sense Finger Deformation or distributed Pressure to Detect Lumps in Soft Tissue?*, Proc. of the ASME Dyn. Sys. and Control Div, Vol. 64, pp 273-278, Anaheim, California, Nov. 1998.
21. J. Silva-Martínez and S. Solís-Bustos, *Design Considerations for High Performance Very ow Frequency Filters*, Proceedings of the 1999 IEEE International Symposium on Circuits and Systems, ISCAS'99, Vol. 2, 1999.
22. A. Veeravalli, E. Sánchez-Sinencio and J. Silva-Martínez, *Transconductance Amplifier Structures With Very Small Transconductances: A Comparative Design Approach*, IEEE Journal of Solid-State Circuits, 2002.